European Journal of Applied Sciences – Vol. 13, No. 02
Publication Date: April 25, 2025
DOI:10.14738/aivp.1302.18604.
Sorescu, M., Nickischer, Z., Tolea, F., Sofronie, M., Kelly, J. C., & Aitken, J. A. (2025). Mechanical Milling and Comprehensive Characterization of Dysprosium Oxide-Hematite Magnetic Ceramic Nanostructures. European Journal of Applied Sciences, Vol - 13(02). 412-426.

Mechanical Milling and Comprehensive Characterization of Dysprosium Oxide-Hematite Magnetic Ceramic Nanostructures

Monica Sorescu
Duquesne University, Department of Physics,
Fisher Hall, Pittsburgh, PA 15282, United States

Zachary Nickischer
Duquesne University, Department of Physics,
Fisher Hall, Pittsburgh, PA 15282, United States

Felicia Tolea
National Institute of Materials Physics,
Bucharest-Magurele, 077125, Romania

Mihaela Sofronie
National Institute of Materials Physics,
Bucharest-Magurele, 077125, Romania

Jordan C. Kelly
Duquesne University,
Department of Chemistry and Biochemistry,
Mellon Hall, Pittsburgh, PA 15282, United States

Jennifer A. Aitken
Duquesne University,
Department of Chemistry and Biochemistry,
Mellon Hall, Pittsburgh, PA 15282, United States

ABSTRACT

Magnetic ceramic nanostructures of the type xDy_2O_3-(1-x) α-Fe_2O_3 (x=0.1 and 0.5) were synthesized by mechanochemical activation for ball milling times of 0, 2, 4, 8 and 12 hours. The 0-h Mössbauer spectrum was analyzed with a sextet characteristic to hematite. A second sextet for x=0.5 and a second and third sextet for x=0.1, with lower values of the hyperfine magnetic field, were assigned to dysprosium-doped hematite. An additional quadrupole-split doublet, whose relative abundance increased with the ball milling time and molar concentration, was assigned to superparamagnetic dysprosium iron perovskite (dysprosium orthoferrite) phase. The X-ray diffraction (XRD) patterns for the molar concentration x=0.5 showed the presence of $DyFeO_3$ peaks after 12 h of milling. The hysteresis loops recorded at 5 K and an applied magnetic field of 5 T exhibited coercive fields that increased with ball milling time, while the hysteresis loops at 300 K were consistent with a strong paramagnetic component. The zero-field-cooling-field-cooling (ZFC-FC) measurements performed at 200 Oe and 5-300 K

showed the effect of milling time on the Morin transition of hematite. The optical diffuse reflectance spectra showed that the samples were semiconductors with a band gap of ~2.1 eV.

Keywords: oxides, Mössbauer spectroscopy, magnetic properties, optical properties.

INTRODUCTION

Hematite (α-Fe_2O_3) has been the focus of various theoretical and experimental studies, owing to its applications as a magnetic, semiconductor and catalytic material. Doping hematite with several transition metal and rare earth elements was found to determine an improvement of its electrochemical and photocatalytical properties [1-6].

Dysprosium oxide (Dy_2O_3) is a paramagnetic compound that can be used to functionalize hematite with prospective applications in sensing, catalysis and flexible electronics. In particular, dysprosium ion Dy^{3+} was found to exhibit intriguing properties when introduced in several systems [7-22]. Thus, magnetite nanoparticles electrochemically doped with dysprosium cations were found to lead to the development of novel iron-based electrodes, due to their supercapacitive and magnetic properties [8]. The Dy^{3+} ion was found to present a combined impact on the physical, optical, magnetic and DC-electrical properties of dysprosium doped $Cu_{0.8}Cd_{0.2}Dy_xFe_{2-x}O_4$ nanoferrites [11]. The effect of Dy replacing Fe on the microstructure, electrical properties and magnetic properties of NiZnCo ferrite was also investigated [12]. Reference [14] reports on the effect of dysprosium substitution on the crystal structure and physical properties of multiferroic $BiFeO_3$ ceramics. A Mössbauer study of multiferroic $DyFeO_3$ is available in literature [16], but the dysprosium orthoferrite investigated was in polycrystalline form rather than nanoparticles.

Recently, the ball milling technique was key to obtaining garnet-graphene nanocomposites [23] and crucial to determine the formation of skyrmion phase in the Fe-Co-Si system [24]. Moreover, mechanochemical activation was used to synthesize mixed-oxide nanostructures of the type xGd_2O_3-(1-x) α-Fe_2O_3 [25] and xNd_2O_3-(1-x) α-Fe_2O_3 [26], with the presence of solid solutions in the former and absence of solid solutions in the latter system.

In the present study we shed light on the structural, magnetic and optical properties of the xDy_2O_3-(1-x) α-Fe_2O_3 system with molar concentration x=0.1 and 0.5, obtained by mechanochemical activation at different ball-milling times. Our investigation aims at determining the phase sequence, mutual solubility, hyperfine, magnetic and optical properties of the mixed oxides as a function of processing parameters and relies on Mössbauer spectroscopy, X-ray diffraction (XRD), magnetic measurements (hysteresis loops and zero-field-cooling-field-cooling, ZFC-FC) and optical diffuse reflectance spectroscopy.

MATERIALS AND METHODS

Nanoparticles of xDy_2O_3-(1-x) α-Fe_2O_3 (x=0.1 and 0.5) were obtained by mechanochemical activation of precursor powders of hematite and dysprosium oxide (Alfa Aesar), with particle sizes in the tens of nanometers range. The powders were mixed manually using a mortar and pestle and introduced in a SPEX 8000 mixer mill. They were ground for time periods ranging from 0 to 12 hours. The powder to ball mass ratio was 1:5.

Transmission Mössbauer spectra were recorded at ambient temperature using a SeeCo constant accelerator spectrometer. A 25 mCi ^{57}Co gamma ray source in a Rh matrix was used. All spectra were deconvoluted by least-squares fitting using the WINORMOS package of programs in the assumption of Lorentzian lineshapes.

The samples were deposited onto a zero-background silicon wafer. Powder X-ray diffraction data were collected using a Malvern Panalytical Empyrean 3 multipurpose powder X-ray diffractometer with an X'cellerator detector operating in Bragg–Brentano geometry and using Cu $K\alpha$ radiation, λ = 1.541871 Å. The tube was energized using 45 kV and 40 mA. Data were collected from 5 to 100° 2θ in steps of 0.0167° at a scan speed of 0.023537° s^{-1}. A 0.04 rad soller slit and a 2° anti-scatter slit were used on the incident side of the beam, while the diffracted beam optics consisted of a 0.04 rad soller slit, a programmable anti-scatter slit, and a nickel filter. Phase identification of crystalline components was carried out using the *X'Pert HighScore Plus* software package and the International Centre for Diffraction Data (ICDD) powder diffraction file (PDF) database.

Magnetic property measurements were performed using a superconductor quantum interference device (SQUID) magnetometer with a 5 T magnetic field for recording the hysteresis loops at 300 and 5 K and a 200 Oe magnetic field for the zero-field-cooling-field-cooling (ZFC-FC) measurements in the 5-300 K temperature range.

Data from 2500 to 200 nm were collected with a Varian Cary 5000 UV–Vis–NIR spectrophotometer coupled with a diffuse reflectance accessory at a rate of 600 nm min^{-1}. The 100% reflectance standard was $BaSO_4$ (Fisher Scientific, 99.92%). The sample was ground and pressed on top of the reference that was preloaded in the sample cup. Reflectance data were converted to absorption by employing the Kubelka–Munk equation.

RESULTS AND DISCUSSION

Mössbauer Spectroscopy

As a high-resolution nuclear technique with applications in solid state physics, Mössbauer spectroscopy was employed in order to obtain local-probe information on the structural and magnetic properties of dysprosium oxide-hematite ceramic nanostructures. Figures 1-2 (a)-(e) show the room-temperature transmission Mössbauer spectra of the xDy_2O_3-(1-x) α -Fe_2O_3 nanoparticles system for molar concentration x=0.1 and 0.5 and ball milling times (BMT) of 0, 2, 4, 8 and 12 hours, respectively. The least-squares fitted values of the Mössbauer parameters are presented in Table 1. The spectra in Figures 1-2 (a) were analyzed by considering one six-line pattern, with the magnetic hyperfine field (B_{hf}) of 50.7 T, characteristic to hematite.

Analysis of the Mössbauer spectra in Figures 1 (b)-(e) for molar concentration x=0.1 required the consideration of two additional sextets, with magnetic hyperfine field values smaller than the value for hematite. These sextets are due to substitutions of Fe^{3+} ions by Dy^{3+} ions in the hematite structure, such that the Dy sites have a lower hyperfine magnetic field than the Fe sites. Consequently, these sextets were assigned to dysprosium-doped hematite. The dependance of the magnetic hyperfine field values of the three sextets on the ball milling time is indicative of the formation of a solid solution in the specimens investigated. Only one additional sextet was necessary to analyze the Mössbauer spectra in Figures 2 (b)-(e) for molar

concentration x=0.5, and this sextet also exhibited a lower value of the magnetic hyperfine field when compared to the value for hematite.

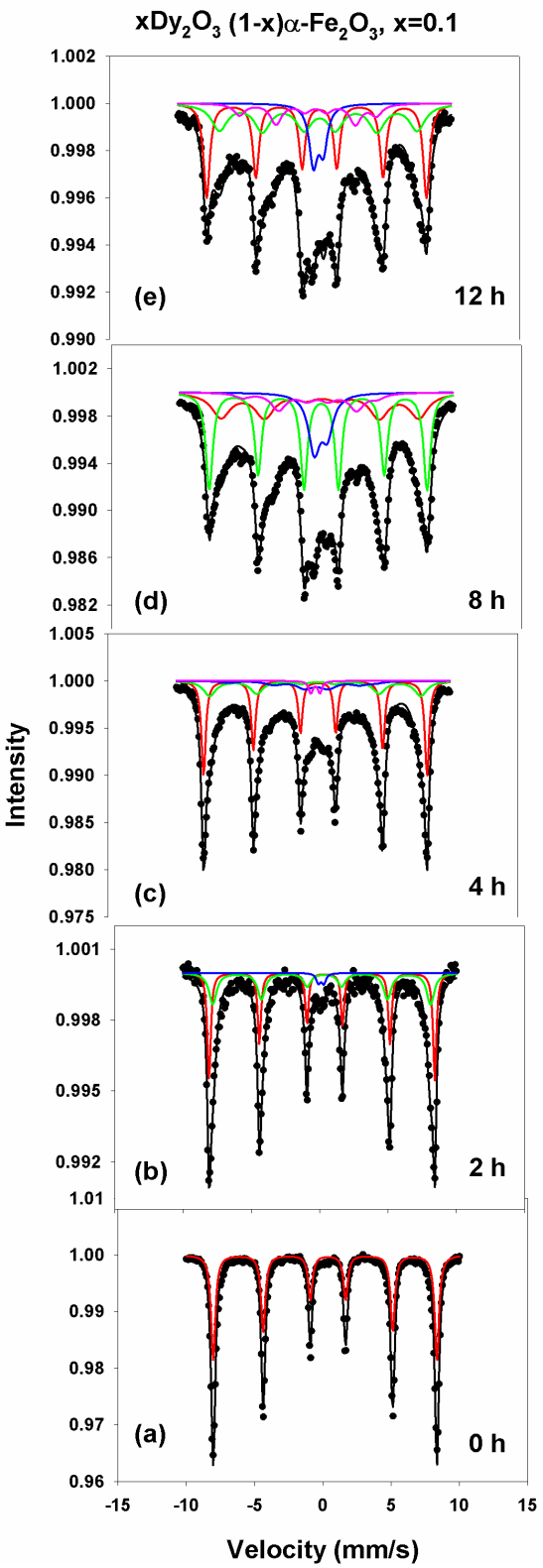

Fig 1: Mössbauer spectra for x=0.1 and BMT of 0-12 h

This result is consistent with the formation of a limited solid solution in the system, due to substitutions of Fe ions by Dy ions, and was assigned to dysprosium-doped hematite. A higher level of substitution did not occur and only a limited solid solution was obtained, due to the difference in ionic radii of the Dy and Fe ions.

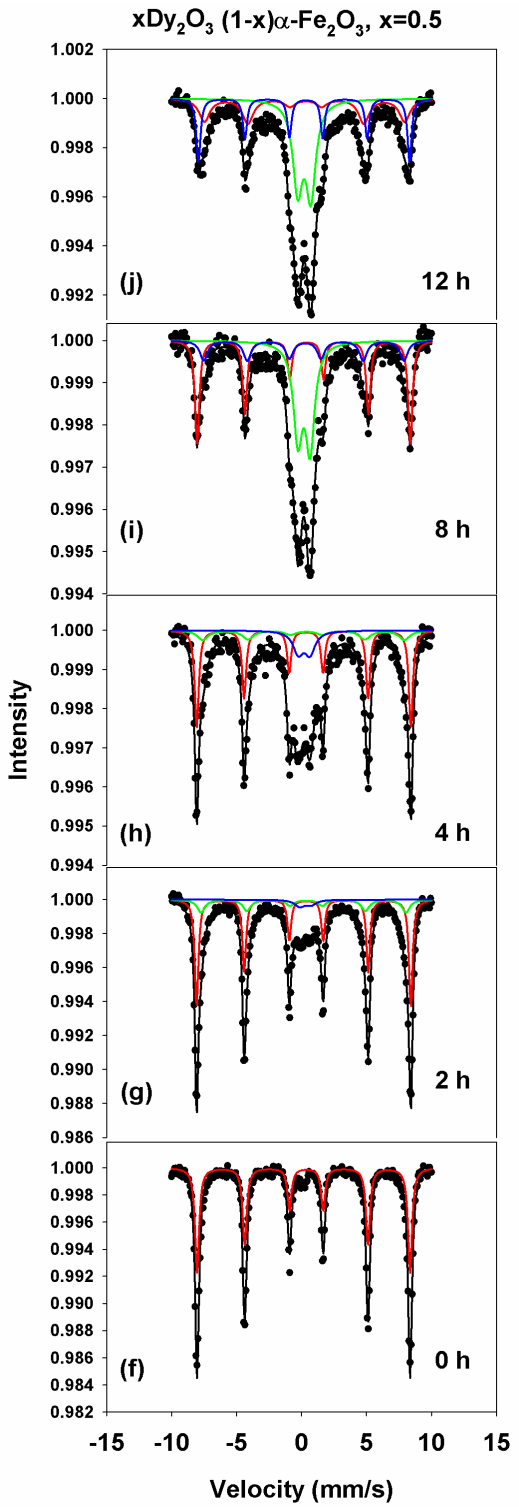

Fig 2: Mössbauer spectra for x=0.5 and BMT of 0-12 h

Thus, the ionic radius of the Dy^{3+} ions with six coordination numbers is 1.052 Å, while that of the Fe^{3+} ions is 0.645 Å. It is, however, interesting to note that the ability to form solid solutions in the dysprosium oxide-hematite system decreases as a function of molar concentration.

An additional quadrupole-split doublet, with a typical quadrupole splitting of 0.4-0.9 mm/s, had to be introduced in the analysis of the Mössbauer spectra in Figures 1 (b)-(e) and 2 (b)-(e).

This doublet was assigned to superparamagnetic dysprosium iron perovskite (dysprosium orthoferrite), $DyFeO_3$. Dysprosium orthoferrite is known to exhibit ferrimagnetism, but in the present study the nanoparticles of dysprosium orthoferrite are too small to be magnetic at room temperature, which gives rise to superparamagnetism. The reduced particle size due to prolonged milling is translated into a quadrupole-split doublet in the Mössbauer spectra.

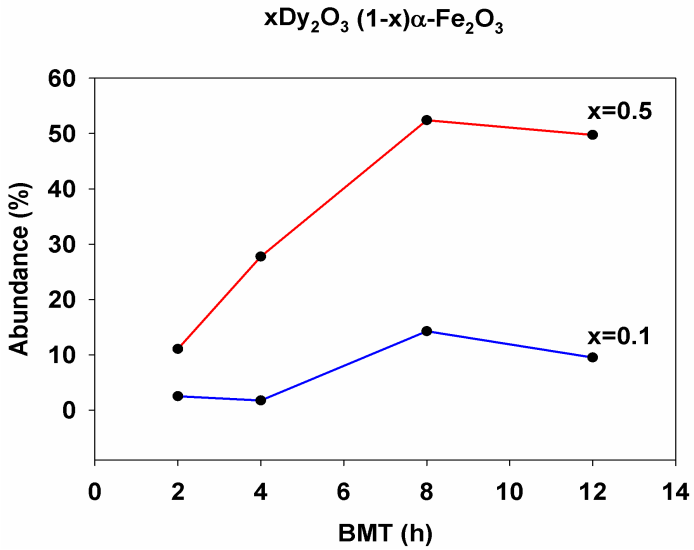

Fig 3: Relative abundance of the doublet for x=0.1 and x=0.5

Figure 3 presents the dependance of the relative abundance of the quadrupole-split doublet as a function of the ball milling time for both values of the molarities used. It can be inferred that the doublet abundance increases with increasing the milling time and reaches 52.41% for the sample with x=0.5 ball-milled for 8 hours. It can be seen from this plot that the production of $DyFeO_3$ is more pronounced at higher molar concentration. The formation of the dysprosium iron perovskite during the mechanical milling process can be modeled by considering the reaction.

$Dy_2O_3+Fe_2O_3 \rightarrow 2DyFeO_3$, which is proposed to occur during the high-energy ball milling performed.

X-ray Diffraction

To complement the Mössbauer spectroscopy investigations on the phase composition of the milled samples, X-ray diffraction (XRD) measurements have also been performed. The XRD patterns of the xDy_2O_3-(1-x) α-Fe_2O_3 nanoparticles system for x=0.5 and ball milling times of 0, 2, 4, 8 and 12 hours, respectively are presented in Figure 4 (a)-(e). The diffractogram in Figure

4 (a) is consistent with diffraction peaks from α-Fe_2O_3 (PDF card 01-089-0598) and Dy_2O_3 (PDF card 01-086-1327) oxides, which correspond to the original starting material before ball milling. It can be inferred that the peaks of the dysprosium perovskite appear (PDF card 01-074-1478) after exposure to mechanochemical activation. The pattern of $DyFeO_3$ peaks dominates the XRD diffractogram after 12 h of exposure to high-energy ball milling. These results are in good, qualitative agreement with the Mössbauer findings presented in the previous section.

Table 1: Mössbauer parameters of the xDy2O3 (1-x) α-Fe2O3 nanoparticles system

x	BMT	δ	2ε	Δ	B_{hf}	Relative areas	Assignment of sites
	(hours)	(mm/s)	(mm/s)	(mm/s)	(T)	(%)	
0.1	0	0.261	-0.216		50.76	100	α-Fe_2O_3
	2	0.267	-0.206		51.22	37.76	α-Fe_2O_3
		0.245	-0.200		49.41	59.72	Dy:Fe_2O_3
		0.109		0.400		2.52	$DyFeO_3$
	4	0.262	-0.203		50.71	31.75	α-Fe_2O_3
		0.257	-0.201		47.91	38.99	Dy:Fe_2O_3
		-0.292	-1.088		33.49	27.51	Dy:Fe_2O_3
		0.162		0.661		1.75	$DyFeO_3$
	8	0.243	-0.220		49.44	28.95	α-Fe_2O_3
		0.328	-0.139		44.90	42.63	Dy:Fe_2O_3
		-0.191	-0.555		30.62	14.14	Dy:Fe_2O_3
		0.324		0.958		14.28	$DyFeO_3$
	12	0.258	-0.214		49.89	24.89	α-Fe_2O_3
		0.328	-0.100		44.89	51.77	Dy:Fe_2O_3
		-0.200	-0.567		31.10	13.81	Dy:Fe_2O_3
		0.280		0.723		9.53	$DyFeO_3$
0.5	0	0.262	-0.214		50.79	100	α-Fe_2O_3
	2	0.262	-0.194		51.08	54.83	α-Fe_2O_3
		0.252	-0.200		48.85	34.12	Dy:Fe_2O_3
		0.293		0.861		11.05	$DyFeO_3$
	4	0.262	-0.178		51.05	40.81	α-Fe_2O_3
		0.264	-0.220		48.06	31.43	Dy:Fe_2O_3
		0.192		0.903		27.76	$DyFeO_3$
	8	0.281	-0.227		50.83	26.31	α-Fe_2O_3
		0.228	-0.105		47.76	21.28	Dy:Fe_2O_3
		0.186		0.939		52.41	$DyFeO_3$
	12	0.257	-0.161		50.34	14.18	α-Fe_2O_3
		0.268	-0.101		47.76	36.08	Dy:Fe_2O_3
		0.195		1.010		49.74	
Errors:		±0.05	±0.05	±0.05	±1.00	±1.00	

Magnetic Measurements

Magnetic measurements were performed to complement the local-probe information obtained by Mössbauer spectroscopy. Characteristic to hematite is the fact that its two magnetic sublattices have equal moment and antiparallel orientation below the Morin temperature, T_M=262 K, for pure hematite [5]. At temperatures higher than the Morin temperature, the two

sublattices are slightly canted, leading to weak ferromagnetism. The magnetic ordering of the weak ferromagnetic type given by uncompensated magnetic moments is present for a large range of temperatures for the sample milled for 12 h, such that the Morin transition takes place over a temperature range of 256 K, while for the samples milled for 2, 4 and 8 h the Morin transition is below 70 K.

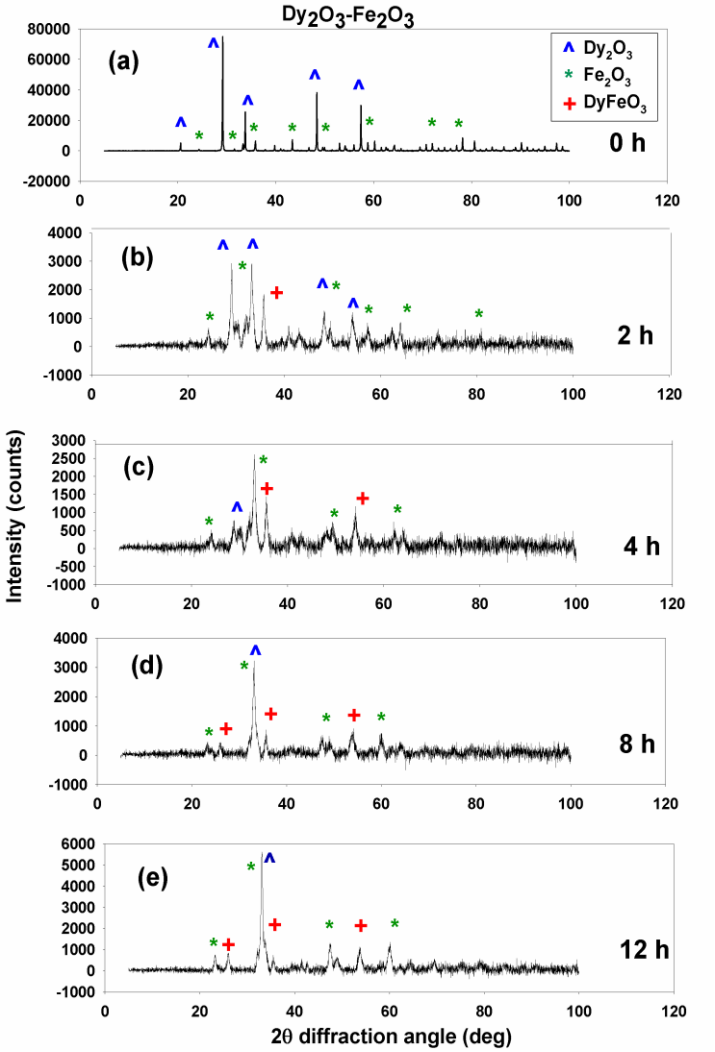

Fig 4: XRD patterns for x=0.5 and BMT of 0-12 h

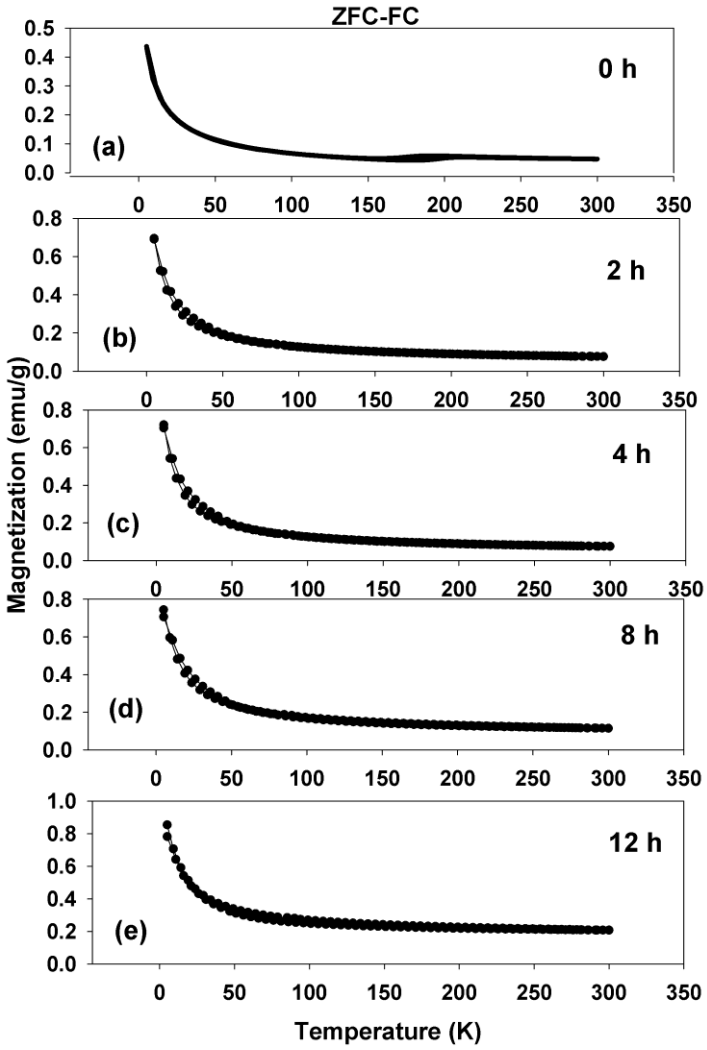

Fig 5: ZFC-FC curves at 200 Oe as a function of BMT.

Figure 5 (a)-(e) presents the zero-field-cooling-field cooling (ZFC-FC) curves recorded in the temperature interval 5-300 K with an applied magnetic field of 200 Oe. These curves show the way in which the milling time influences the Morin temperature. The 0-h sample presents a hysteresis in temperature described by magnetization as an effect of heating and cooling of the sample. This hysteresis is associated with the Morin transition, which occurs in the temperature range of 152 K to 212 K for the 0-h sample. After 2-h milling time, this hysteresis occurs at lower temperatures, between 5 K and 70 K. A similar behavior is shown by the 4-h milled sample, for which the Morin transition takes place between 6 K and 60 K. After 8 h of milling time, the Morin transition occurs between 7 K and 52 K, while after 12 h of milling, the Morin transition takes place over a much larger temperature range, between 24 K and 280 K. This behavior is likely due to a change in spin reorientation in Dy: α-Fe_2O_3 and Fe:Dy_2O_3.

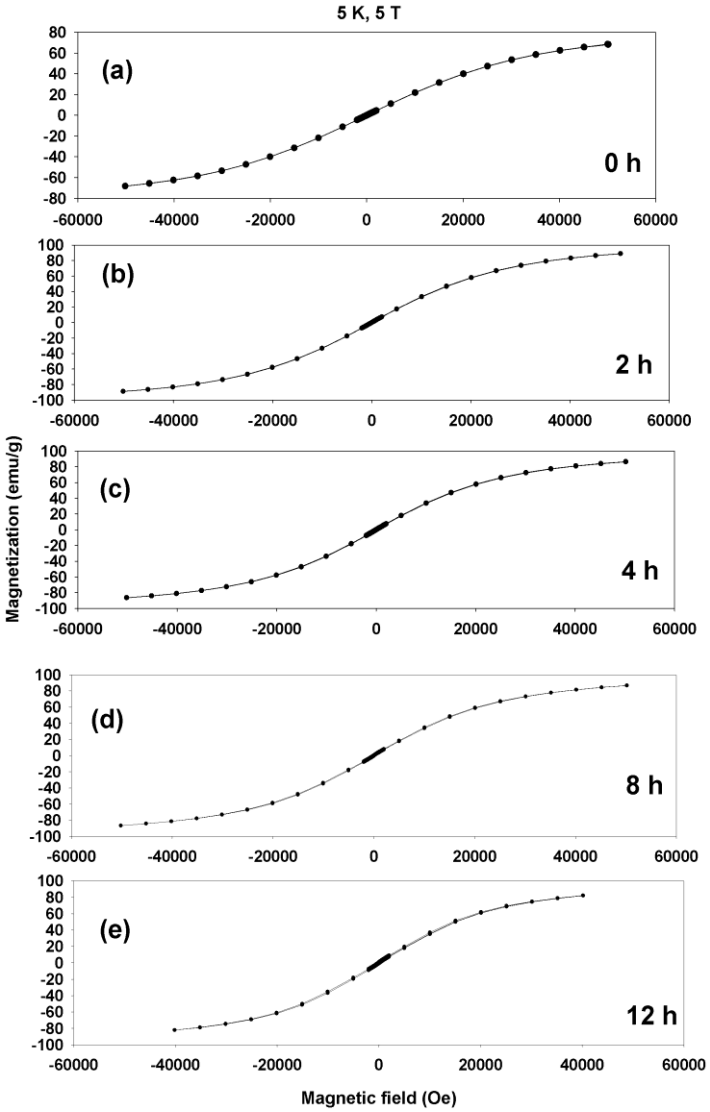

Fig 6: Hysteresis loops at 5 K and 5 T as a function of BMT.

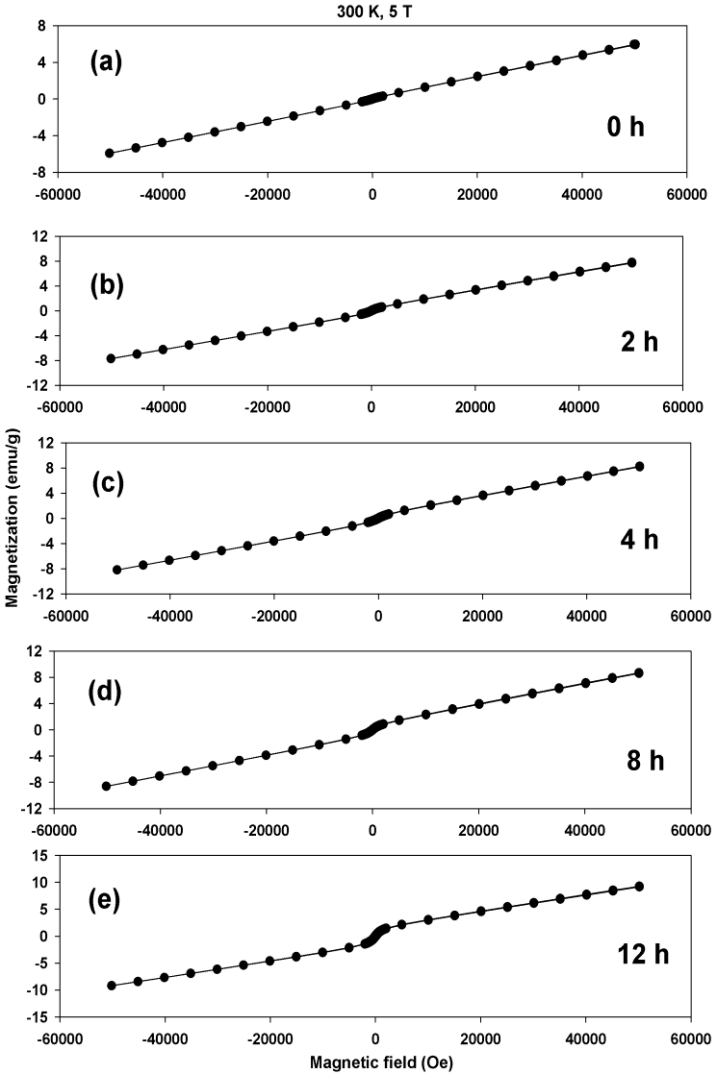

Fig 7: Hysteresis loops at 300 K and 5 T as a function of BMT.

It may also be noted that the values of magnetization are small, as there are not many uncompensated magnetic moments and the antiferromagnetic ordering prevails. The magnetization increases with milling time and this is supported by the ZFC-FC as well as hysteresis loop measurements. Figures 6 and 7 (a)-(e) show the hysteresis loops recorded at 5 K and respectively, 300 K with an applied magnetic field of 5 T (1T=10,000 Oe) for the equimolar composition samples (x=0.5), ball-milled for 0-12 h. The hysteresis loops show that magnetization does not saturate in the applied magnetic field of 5 T, neither at 5 K, nor at 300 K, and this is true for all samples. As can be seen in Table 2, the coercive field at 5 K (taken as the average of H_{c+} and H_{c-}) increases with milling time, while at 300 K there is no clear trend in the coercivity values. It is also important to note that the 300 K hysteresis loop presents a strong paramagnetic component.

The values of the exchange bias field H_{eb} were also calculated from the H_{c+} and H_{c-} data and listed in Table 2. These values are very small: at 5 K only the 12-h sample has a H_{eb} of 22.75 Oe, while at 300 K the 8-h milled sample has an H_{eb} of -19.5 Oe. The results of magnetic

measurements show that the values of the magnetic parameters can be controlled by the ball milling time employed.

Table 2: Positive, negative and average coercive fields and exchange bias field of the Dy_2O_3-Fe_2O_3 nanoparticles system at 5 and 300 K as a function of milling time

T (K)	BMT (h)	H_{c-} (Oe)	H_{c+} (Oe)	$<H_c>$ (Oe)	H_{eb} (Oe)
	0	-7.3	8	7.65	0.35
	2	-13.3	11.5	12.4	-0.9
	4	-54	53	53.5	-0.5
	8	-100	96.6	98.3	-1.7
	12	-160	205.5	182	22.75
300	0	-103	102	102.5	-0.5
	2	-113	109	111	-2.0
	4	-122	97	109.5	-12.5
	8	-106	67	86.5	-19.5
	12	-93	91.7	92.35	-0.65
Errors:		±0.1	±0.1	±0.1	±0.1

Optical Diffuse Reflectance Spectroscopy

In order to characterize the optical property changes induced by mechanochemical activation in the dysprosium oxide-hematite system, optical diffuse reflectance spectroscopy (ODRS) measurements were also undertaken in the present study. Figure 8 (a) shows the optical absorption spectra of the dysprosium oxide-hematite equimolar mixture as a function of energy over the UV-VIS-NIR spectral range for all milling times employed. For the starting material, hematite has a band gap of 1.9-2.2 eV in the visible region, while the dysprosium oxide exhibits absorption bands primarily in the UV region, with characteristic peaks around 3.35 and 3.49 eV, corresponding to transitions from the ground state to various excited states [27]. For the ball-milled material, it can be seen that absorbance is considerably enhanced and broadened, an effect we believe to result from the substitution of Dy ions for Fe.

According to Tauc plots, the dependence of $(\alpha E)^2$ as a function of energy (eV) is able to yield the band gap of the compound [28, 29]. The exponent of 2 was chosen because the 2.2 eV transition in hematite is indirect. Indeed, it can be observed in Figure 8 (b) that the intercepts give a value of ~2.1 eV for the band gap. This value is independent of the milling time employed. Indeed, it can be seen in this figure that there is no absorption below 2.1 eV for all milling times, while above the band gap there is a broad absorption that depends on the milling time employed. These results show that the dysprosium oxide-hematite mixed-oxide nanostructures have semiconductor properties.

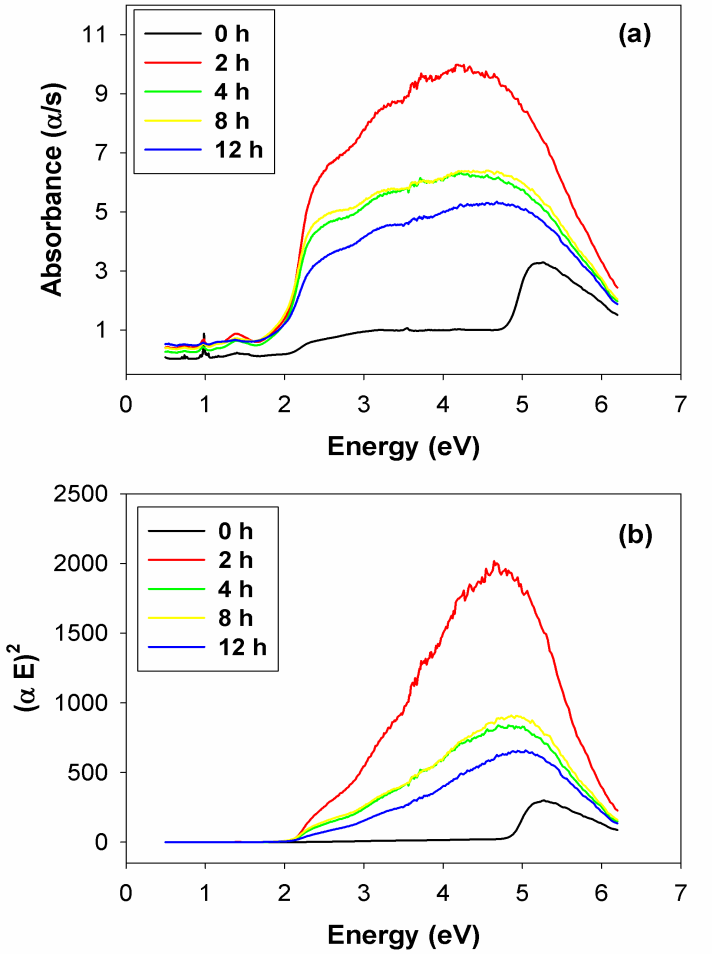

Fig 8: Optical diffuse reflectance spectra for x=0.5 as a function of BMT.

CONCLUSIONS

The main results of the present study can be summarized as follows:

1. Mixed oxide nanostructures of the type xDy2O3-(1-x) α-Fe2O3 were successfully synthesized by high energy ball milling for molar concentrations x=0.1 and 0.5.
2. XRD patterns support the formation of dysprosium doped hematite and dysprosium orthoferrite at long milling times.
3. The Mössbauer spectra reveal the formation of solid solutions in the milled specimens.
4. Magnetic measurements demonstrate an increase in coercivity with ball milling time at 5 K and the presence of a strong paramagnetic component at 300 K. The ZFC-FC data show the effect of the milling time on the Morin transition temperature of hematite.
5. The ODRS optical spectra present an increased and broadened absorption with ball milling time and demonstrate that the mixed oxides are semiconductors with a band gap of ~2.1 eV.

ACKNOWLEDGMENT

This work was supported in part by the National Science Foundation, USA under grants number DMR-0854794 and DMR-1002627-1. Funding was also received from the Ministry of Research, Innovation and Digitization (Romania), CNCS/CCCDI-UEFISCDI core program under projects

PC2-PN23080202 and 35PFE/2021. J.A.A. and J.C.K. acknowledge the support of the National Science Foundation, USA under grant DMR-1611198. The X-ray powder diffractometer was purchased with funds from the National Science Foundation, USA (DUE-0511444) and an upgrade was financed by the Bayer School of Natural and Environmental Sciences at Duquesne University.

Conflict of Interests

There are no conflicts of interests regarding the work described in this paper.

References

1. Rozenberg, G.Kh., et al., High pressure structural studies of hematite Fe2O3, Physical Review B, 2002. 65: 064112.

2. Bergenmayer, W., et al., Ab Initio thermodynamics of oxide surfaces: O2 on Fe2O3 (0001), Physical Review B, 2004. 69: 195409.

3. Zheng, Y., et al., Quasicubic□□-Fe2O3 nanoparticles with excellent catalytic performance, Journal of Physical Chemistry B, 2006. 110: p. 3093-3097.

4. Wu, C., et al., Synthesis of hematite (□-Fe2O3) nanorods: Diameter-size and shape effects on their applications in magnetism, lithium ion battery, and gas sensors, Journal of Physical Chemistry B, 2006. 110: p.17806-17812.

5. Liu, J.Z., Morin transition in hematite doped with Iridium ions, Journal of Magnetism and Magnetic Materials, 1986. 54-57: p. 901-902.

6. Stroh, C., et al., Ruthenium oxide-hematite magnetic ceramics nanostructures, Ceramics International, 2015. 41: p. 14367-14375.

7. Wu, Y., et al., Phase evolution and microstructure characteristics of Mo-based Tb2O3-Dy2O3 composites synthesized by ball milling and sintering, Advanced Powder Technology, 2018.29: p.359-366.

8. Aghazadeh, M., et al., Evaluation of supercapacitive and magnetic properties of Fe3O4 nanoparticles electrochemically doped with dysprosium cations: Development of a novel iron-based electrode, Ceramics International, 2018.44: p.520-529.

9. Balg, M.M., et al., Surfactant assisted synthesis of rare earth Dy3+ substituted MnFe2O4 nanoparticles, Ceramics International, 2019.45: p.18014-18022.

10. Padmasree, G., et al., Study of structural, electrical and hyperfine properties of Dy doped YFeO3, Ceramics International, 2022.48: p.28980-28985.

11. Vinod, G., et al., Dysprosium doped Cu0.8Cd0.2DyxFe2-xO4 nano ferrites: A combined impact of Dy3+ on enhanced physical, optical, magnetic and DC-electrical properties, Ceramics International, 2023.49: p.2829-2851.

12. Huang, S.J., et al., Effect of Dy replacing Fe on microstructure, electrical properties, and magnetic properties of NiZnCo ferrite, Ceramics International, 2023.49: p.22204-22210.

13. Hashim, M., et al., Structural, optical, elastic and magnetic properties of Ce and Dy doped cobalt ferrites, Journal of Alloys and Compounds, 2020.834: p.155089.

14. Koval, V., et al., Effect of dysprosium substitution on crystal structure and physical properties of multiferroic BiFeO3 ceramics, Journal of the European Ceramic Society, 2014.34: p.641-651.

15. Almessiere, M.A., et al., Strong correlation between Dy3+ concentration, structure, magnetic and microwave properties of the [Ni0.5Co0.5] (Dy_xFe_{2-x}) O_4 nanosized ferrites, Journal of Industrial and Engineering Chemistry, 2020.90: p.251-259.

16. Reddy, S.S.K., et al., Structural, electrical, magnetic and 57Fe Mössbauer study of polycrystalline multiferroic DyFeO3, Journal of Magnetism and Magnetic Materials, 2015.396: p.214-218.

17. Kumar, H., et al., Structural and magnetic study of dysprosium substituted cobalt ferrite nanoparticles, Journal of Magnetism and Magnetic Materials, 2016.401: p.16-21.

18. Rahimi, H., et al., The role of dysprosium on the structural and magnetic properties of (Nd1-xDyx)2Fe14B nanoparticles, Journal of Magnetism and Magnetic Materials, 2017.424: p. 199-206.

19. Kumar, P., et al., Role of dysprosium doping concentration on structural deformation of zin oxide nanoparticles, Physica B, 2021.621: p.413313.

20. Korkmaz, A.D., Intrinsic magnetic-optical features of Dy3+ ion substituted NiCuZn nanospinel ferrites via sonochemical approach, Physica B, 2023.654: p.414741.

21. Garcia-Martinez, G., et al., Phase evolution induced by mechanical milling in Ln2O3:TiO2 mixtures (Ln=Gd and Dy), Powder Technology, 2005.152: p.72-78.

22. Lv, D., et al., Ball milling and sintering of neutron absorber Mo-based Tb2O3-Dy2O3 composite and its characterization, Powder Technology, 2018.331: p.226-235.

23. Glasser, S., et al., Effects of mechanochemical activation on the structural, magnetic and optical properties of yttrium iron garnet-graphene nanoparticles, Physica B, 2023. 650: 414501.

24. Sorescu, M., et al., Formation of skyrmion phase in the Fe-Co-Si system by mechanochemical activation, Physica B, 2024. 688: 416153.

25. Glasser, S., et al., Synthesis and characterization of gadolinium oxide-hematite magnetic ceramic nanostructures, Journal of Minerals and Materials Characterization and Engineering, 2023. 11: p. 1-15.

26. Sorescu, M., et al., Mechanochemical synthesis and Mössbauer characterization of neodymium oxide-hematite magnetic ceramic nanoparticles: Phase sequence and recoilless fraction, Materials Chemistry and Physics, 2022. 277: 125511.

27. Aljewaw, O.B., et al., Impact of Dy2O3 substitution on the physical, tructural and optical properties of lithium-aluminium-borate glass system, Applied Sciences, 2020. 10: 10228183.

28. Tauc, J., et al., Optical properties and electronic structure of amorphous germanium, Physica Status Solidi, 1966. 15: p. 627.

29. Mallick, P. and Dash, B.N., X-ray diffraction and UV-Visible characterizations of α-Fe2O3 nanoparticles annealed at different temperature, Nanoscience and Nanotechnology, 2013. 3: p. 130-134.